scientific reports

Check for updates

OPEN

Schisandrin B targets CDK4/6 to suppress proliferation and enhance radiosensitivity in nasopharyngeal carcinoma by inducing cell cycle arrest

Yanhua Fang[1,2], Xinhui Lv[2], Ge Li[3], Piao Wang[2,4], Lingling Zhang[2,5], Ruoyu Wang[2], Lingyun Jia[1]✉ & Shanshan Liang[2]✉

Nasopharyngeal carcinoma (NPC) is notably prevalent in East and Southeast Asia, where despite advancements in radiotherapy leading to high control rates, challenges like radioresistance and collateral tissue damage remain significant. While Schisandrin B (SchB) has been demonstrated antitumor effects in various tumors, its efficacy in NPC remains unexplored. In this study, we explored the antitumor potential of Sch B on NPC, particularly its effects on cell proliferation and radiosensitivity. Our research demonstrates that Sch B effectively inhibits the proliferation of NPC cell lines HONE-1 and CNE-1 by inducing cell cycle G1 phase arrest, specifically through the down-regulation of cyclin-dependent kinase 4/6, without impacting the normal nasopharyngeal epithelial cell line NP69. This selective inhibitory effect positions Sch B as a targeted therapeutic agent, sparing healthy tissue from adverse effects. Furthermore, we observed that Sch B enhances the efficacy of radiotherapy in NPC cells by obstructing DNA double-strand break repair mechanisms, suggesting that a combined treatment regimen of Sch B and radiation could offer a superior therapeutic strategy. These findings propose Sch B not only as a potent inhibitor of NPC cell proliferation but also as an enhancer of radiosensitivity, providing a promising avenue for improving NPC treatment outcomes.

Keywords Schisandrin B, Nasopharyngeal carcinoma, Cell proliferation, Radiosensitivity, CDK4/6

Nasopharyngeal carcinoma (NPC) is an epithelial carcinoma originating from the nasopharyngeal mucosal lining and particularly prevalent in East and Southeast Asia[1]. Radiotherapy is the primary treatment for NPC[2]. Although the 5-year control rate of nonmetastatic NPC by radiotherapy can reach 80–90%, the challenges of radiation resistance and damage to surrounding normal tissues remain significant issues in clinical practice[2,3]. Radiosensitizers are chemical compounds designed to increase the sensitivity of tumors to ionizing radiation so as to reduce damage of surrounding normal tissues. Natural small-molecule compounds often exhibit bidirectional beneficial effects in reducing radiation damage and enhancing immunity, making them an ideal source of radiosensitizers[4,5].

Schisandrin B (SchB), a natural small-molecule compound isolated from *Schisandra chinensis* (Turcz.) Baill., has been widely reported for its neuroprotective, liver protection, antioxidant, anti-inflammatory, antiviral, and anti-tumor effects[6–9]. In recently years, the antitumor effects of Sch B have received increasing attention, with studies reporting its efficacy in colorectal cancer, breast cancer, lung cancer, etc.[10–18]. Its inhibition effects on cancer involve several biological mechanisms, with induction of cell cycle arrest and apoptosis being among the most frequently authenticated[19]. However, the application of Sch B in NPC has not been investigated to date. Besides, Sch B has shown its potential as a chemotherapeutic drug sensitizer that promoted doxorubicin-induced

[1]Liaoning Key Laboratory of Molecular Recognition and Imaging, School of Bioengineering, Dalian University of Technology, Dalian 116024, China. [2]The Key Laboratory of Biomarker High Throughput Screening and Target Translation of Breast and Gastrointestinal Tumor, Affiliated Zhongshan Hospital of Dalian University, No.6 Jiefang Street, Zhongshan District, Dalian 116001, Liaoning, China. [3]Department of Oncology, Dalian Hospital of Traditional Chinese Medicine, No.321 Jiefang Street, Zhongshan District, Dalian 116013, Liaoning, China. [4]Department of Oncology, Central Hospital of Liwan, Guangzhou 510170, China. [5]Department of Radiation Oncology, Fujian Medical University Union Hospital, Fuzhou 350001, China. ✉email: lyjia@dlut.edu.cn; liangshanshan@dlu.edu.cn

apoptosis of breast and hepatic tumor cells without affecting normal cells[20]. Previous studies have demonstrated that Sch B could enhance the efficacy of 5-Fluorouracil (5-FU) chemotherapy in gastric cancer cells[21] and the intensify restriction of docetaxel (DTX)-induced cervical cancer cell growth[22]. This prompts the intriguing question of whether it exhibits similar potential as a radiosensitizer to increase the effectiveness of radiotherapy.

In this study, we first explored the antitumor effect of Sch B on NPC, and the results demonstrated that Sch B could significantly inhibit the proliferation of HONE-1 and CNE-1 cells in vitro, through a mechanism associated with CDK4/6 regulated cell cycle. More importantly, at a concentration of 40 μM, Sch B exhibited significant killing efficiency against NPC cells without affecting the proliferation and cell cycle of normal nasopharyngeal epithelial cells NP69. Besides, our study demonstrated that Sch B augmented the antitumor activity of radiation by delaying the repair of radiation-induced DNA double-strand breaks. This study suggests that combining radiation with Sch B is an effective therapeutic strategy for preventing NPC progression.

Results

Sch B suppresses cell proliferation in NPC cells in vitro but not normal nasopharyngeal epithelial cell

Due to the reported mechanisms of Sch B on other tumors are mainly focused on inhibiting cell proliferation, we first investigated the effects of Sch B on NPC and normal nasopharyngeal epithelial cell proliferation through CCK-8 cytotoxicity-proliferation assay and colony formation assay. The results showed that Sch B inhibited the proliferation of NPC cell line HONE-1, which was time and dose dependent. With the increase of time and concentration of Sch B, the proliferation inhibition of HONE-1 cells gradually increased, and IC50 values of 24, 48 and 72 h were 68.49, 39.10 and 40.95 μM, respectively (Fig. 1A). In another NPC cell line CNE-1, Sch B exhibited the similar inhibitory effect. The IC50 values of 24, 48 and 72 h were 76.75, 42.26 and 44.09 μM, respectively (Fig. 1A). However, Sch B showed low toxicity to the normal cell of NP69, basically no killing effect was observed at the concentration below 40 μM (lg1.4 μM) (Fig. 1A). Microscopy cell counting demonstrated that the number of HONE-1 and CNE-1 cells decreased after 48 h treatment with 40 μM and 80 μM (lg1.6 μM) of Sch B, and the cell morphology changed at 80 μM, compared to 0 μM group (Fig. 1B). However, the number and morphology of NP69 cells substantially unchanged with 40 μM and 80 μM of Sch B (Fig. 1B), though cell viability reduced 40% at 80 μM, 48 h (Fig. 1A), suggesting that Sch B may induce metabolic stress in NP69 cells at higher concentrations without significantly altering cell morphology or number. The results of colony formation assay showed that Sch B inhibited the colony formation ability of HONE-1 and CNE-1 cells in a dose-dependent manner (Fig. 1C,D). These results showed that Sch B suppress NPC cell proliferation in vitro, while having negligible effect on normal nasopharyngeal epithelial cells.

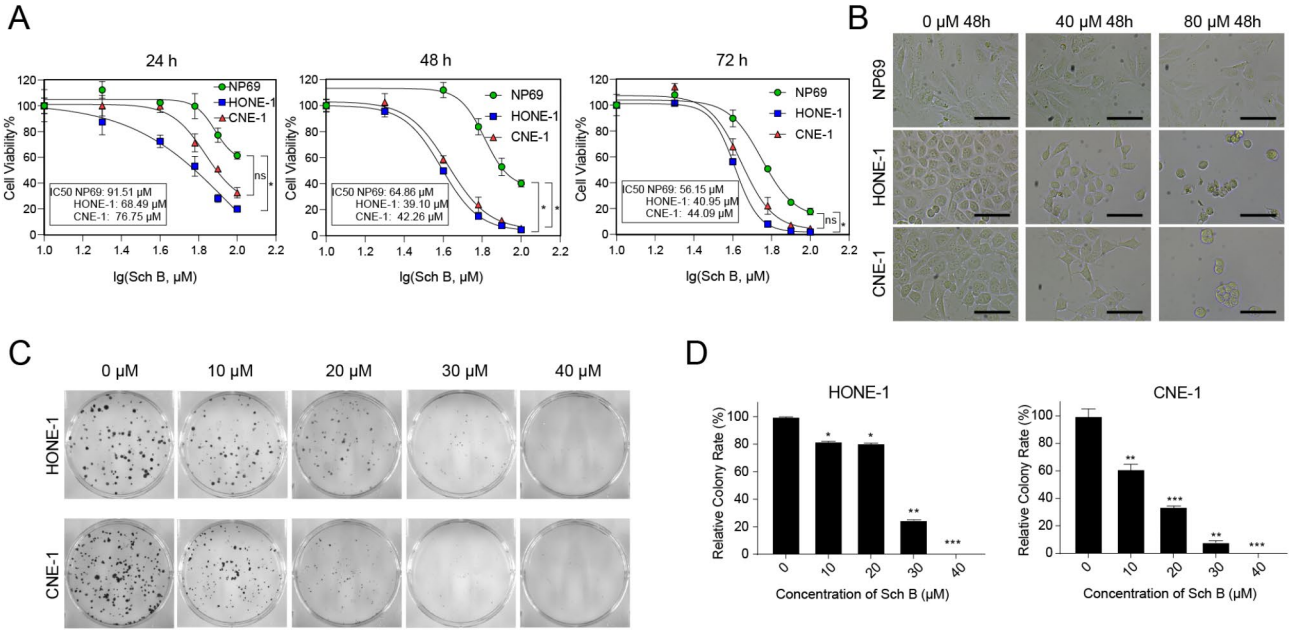

Fig. 1. Sch B suppresses cell proliferation in NPC cells in vitro but not normal nasopharyngeal epithelial cell. (**A**) Cell viability of NPC cells (HONE-1 and CNE-1) and normal nasopharyngeal epithelial cell NP69 treated with 0, 20, 40, 60, 80 and 100 μM Sch B for 24 h, 48 h, 72 h. (**B**) The growth state of HONE-1, CNE-1 and NP69 cells treated with 0, 40, 80 μM Sch B at 48 h (scale bar 200 μm). (**C**,**D**) Colony forming assay for HONE-1 and CNE-1 cells treated with 0, 10, 20, 30, 40 μM Sch B. The colony number was normalized to the 0 μM group. All data are presented as mean ± SD from three independent experiments. $^{*}P < 0.05$; $^{**}P < 0.01$; $^{***}P < 0.001$.

Cell cycle contributes to Sch B-induced NPC cell proliferation inhibition

To further explore the possible mechanism of Sch B in NPC, we analyzed the differential expression genes (DEGs) KEGG pathway in HONE-1 cells with/without Sch B treatment (HONE-1_Sch B/HONE-1). To clarify the pathway with the greatest difference in the effects of Sch B on NPC and normal cells, we also performed the KEGG pathway enrichment on HONE-1 and NP69 cells treated with Sch B (HONE-1_Sch B/NP69_Sch B). The results showed that the effect of Sch B on HONE-1 (HONE-1_Sch B/HONE-1) and the most different effect of Sch B on HONE-1 and NP69 (HONE-1_Sch B/NP69_Sch B) were closely correlated with the cell cycle (Fig. 2A,B). Heatmap cluster analysis of 122 cell cycle enrichment genes showed that HONE-1 cells highly expressed G1 and S phase related genes including CDK4, CDK6, Cyclin D1, and Cyclin E1, compared with NP69 (Fig. 2C). We further performed heatmap on the expression levels of these proteins of interest, allowing for a clearer determination of the differences between groups thus more clearly (Fig. 2D). After treating with Sch B, the expressions of cell cycle related proteins in HONE-1_Sch B cells were approaching to NP69 cells (Fig. 2C,D). Therefore, the proliferation inhibition in NPC cells induced by Sch B was related to cell cycle regulated by CDK and Cyclin proteins.

Sch B induces cell-cycle arrest at G1 phase of HONE-1 and CNE-1 cells, but not normal nasopharyngeal epithelial cell NP69

To further validate the results of RNA-seq that Sch B inhibits NPC proliferation by regulating cell cycle, we performed flow cytometry. The results showed that with the increase of Sch B concentration (10–40 μM), the proportion of HONE-1 and CNE-1 cells in G1 phase significantly increased, while the cycle distribution of normal nasopharyngeal epithelial cell NP69 was not affected by Sch B within this concentration range (Fig. 3A–C). This indicated that Sch B induced cell-cycle of NPC cells arresting at G1 phase. Therefore, we detected the expression of G1 phase related proteins. Western blot results showed that Sch B down-regulated CDK4/6 and up-regulated Cyclin D1 of HONE-1 and CNE-1 cells, but not affecting these proteins in NP69 (Fig. 3D).

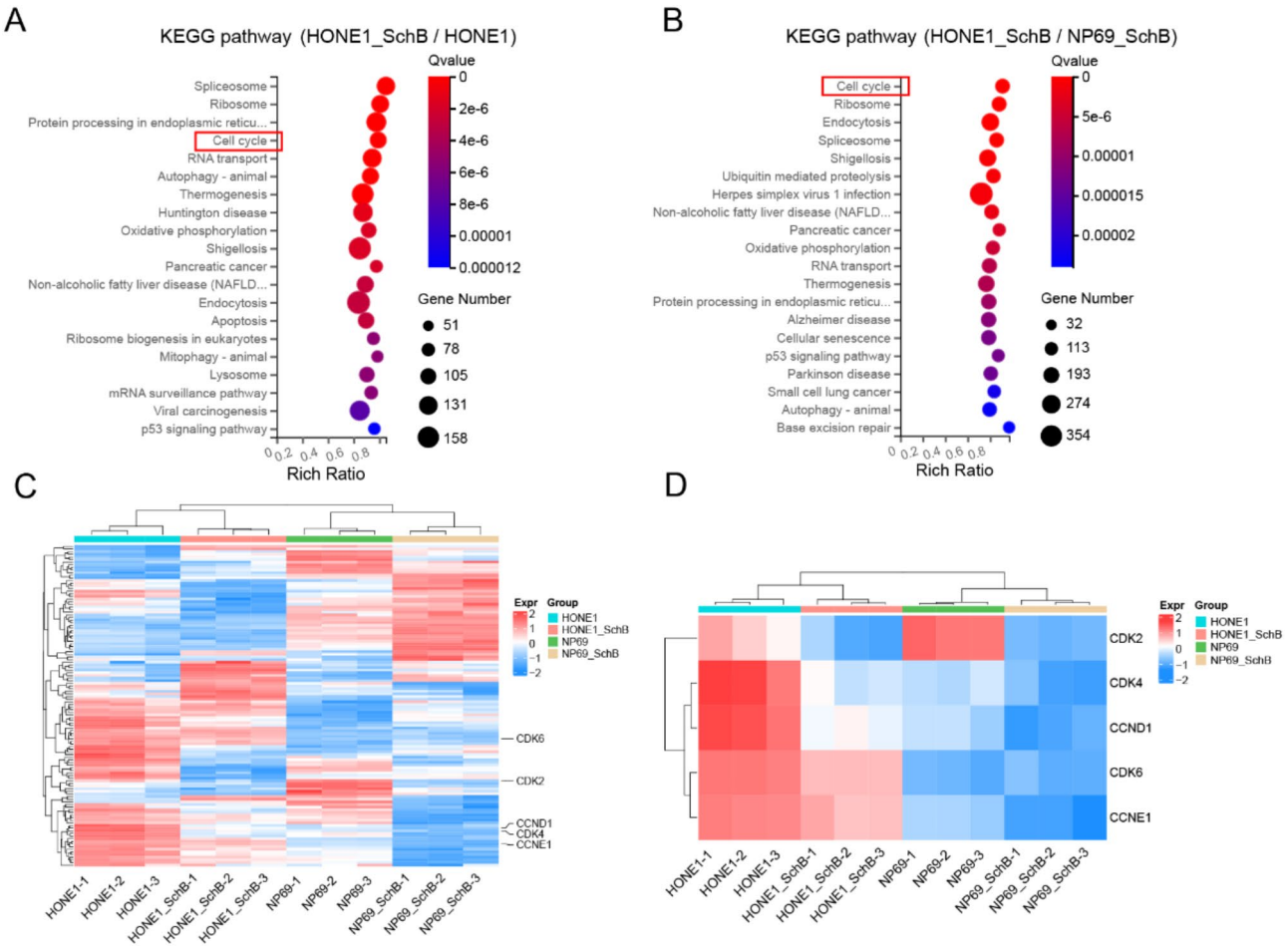

Fig. 2. Cell cycle contributes to Sch B-induced NPC cell growth inhibition. (**A**) The top 20 enriched KEGG pathways of differentially expressed genes of HONE-1_Sch B/HONE-1. (**B**) The top 20 enriched KEGG pathways of differentially expressed genes of HONE-1_Sch B/ NP69_Sch B[23–25]. (**C**) The heat-map analysis of 122 cell-cycle related gene expression in HONE-1, HONE-1_Sch B and NP69. (**D**) The heatmap of gene expression of CDK2, CDK4, CDK6, Cyclin D1, Cyclin E1.

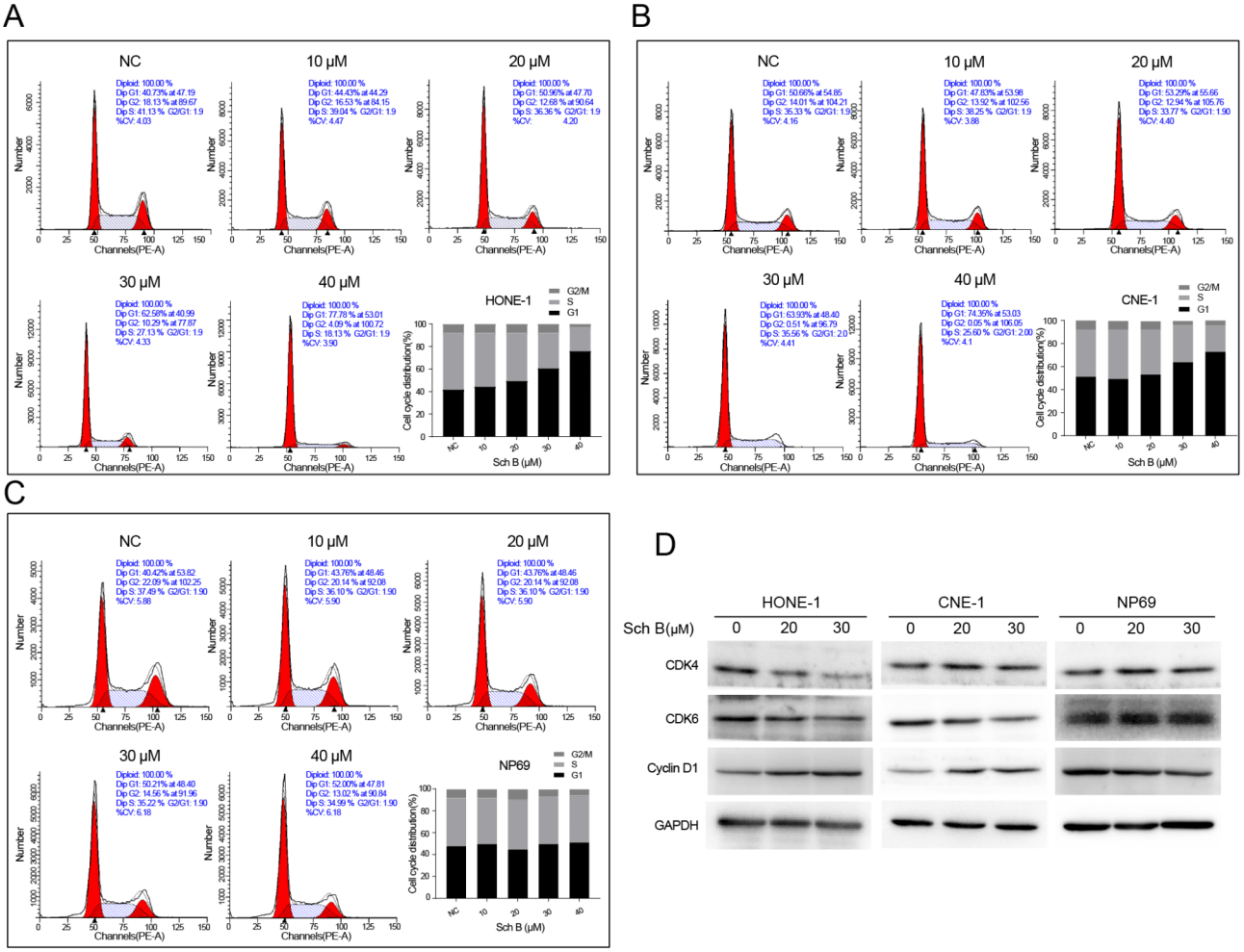

Fig. 3. Sch B induces cell-cycle arrest at G1 phase of HONE-1 and CNE-1 cells, but not normal nasopharyngeal epithelial cell NP69. (**A**–**C**) Flow cytometry of cell cycle distribution in HONE-1, CNE-1 and NP69 cells treated with 0, 10, 20, 30, 40 μM Sch B. (**D**) Immunoblot analysis of CDK4, CDK6, Cyclin D1, protein levels in HONE-1, CNE-1 and NP69 cells treated with 0, 20, 30 μM Sch B. GAPDH was used as a loading control.

Sch B targets CDK4/6 to induce cell-cycle arresting at G1 phase

To explore whether Sch B can directly bind to CDK4/6, Cellular Thermal Shift Assay (CETSA) was conducted. It is an experiment that could detect the binding efficiency of intracellular drugs to target proteins. In general, target proteins would become stable when it binds to drugs, and the proteins degenerate when the temperature increase. If the protein and drug bind at the same temperature, the amount of non-degraded protein will increase[26]. The CETSA results showed that the levels of CDK4 and CDK6 in HONE-1 and CNE-1 cells treated with Sch B increased compared to their respective control group cells across the most temperature conditions. Sch B enhanced the thermal stability of CDK4/6 proteins, indicating that Sch B could directly bind to CDK4 and CDK6 proteins (Fig. 4A). The binding abilities of Sch B with CDK4 and CDK6 were further verified by molecular docking (Fig. 4B). Schematic diagrams of drug-target binding mode are displayed on the right, and the details are on the left. Based on analysis (Autodock 4.2.6), the binding energy of Sch B with CDK4 and CDK6 were − 4.73 and − 5.00 kcal/mol, characterized by hydrogen bonding with amino acid residues in ASP-94 and ARG-44. It suggested that Sch B and CDK4/6 have a certain binding ability.

Sch B increases the sensitivity of NPC cells to radiation

2D HONE-1 and CNE-1 cells were treated with Sch B, radiation, and Sch B combined radiation. After 5 d of culture, cells were fixed and dyed (Fig. 5A,B). The formation rate of clone in the combined treated group was significantly reduced compared to the Sch B group and the radiation group in both HONE-1 and CNE-1 (Fig. 5C). The result suggested that Sch B increased radiosensitivity in NPC cells. The main type of DNA damage induced by radiation is double-strand breaks, and the high capacity for DNA double-strand breaks repair is the most important mechanisms for tumor cell resistance to radiotherapy. We examine γ-H2AX by immunofluorescence to demonstrate and quantify DNA damage in HONE-1 and CNE-1 cells which were prepared with Sch B and radiation. As shown in Fig. 5D–F, 4 h after 4 Gy radiation, the γ-H2AX immunocytochemical positivity in Sch

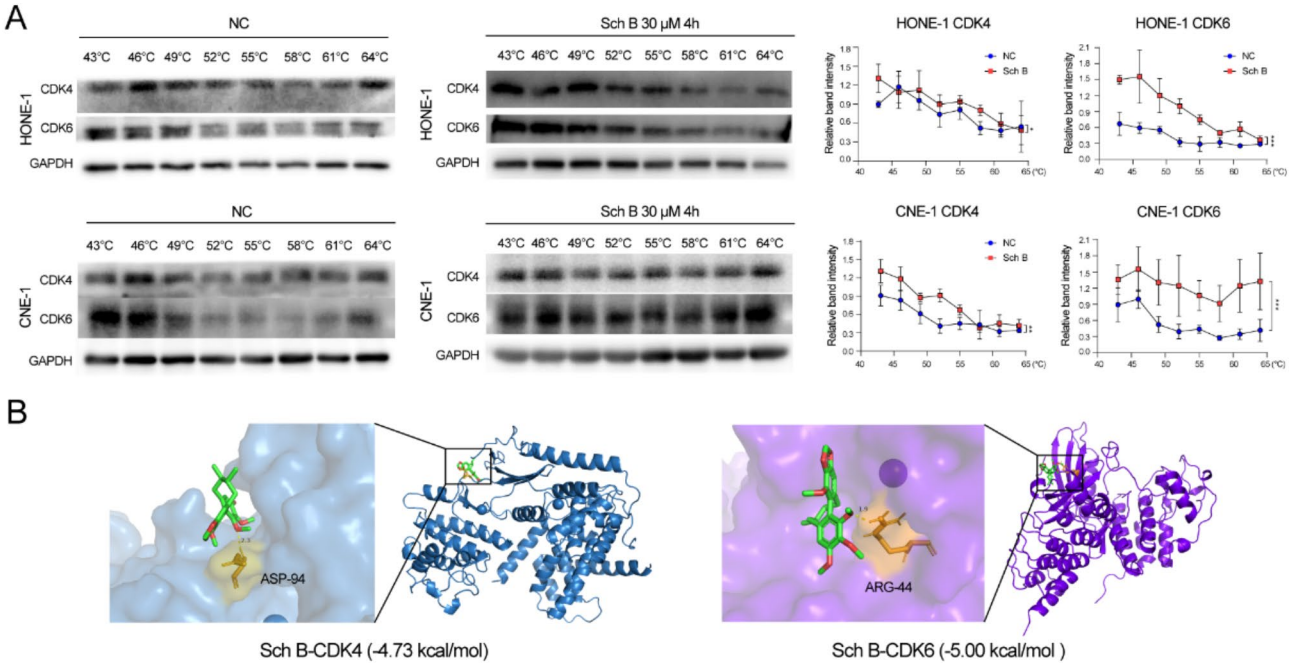

Fig. 4. Sch B targets CDK4/6 to induce cell-cycle arresting at G1 phase. (**A**) Cellular thermal shift assay for HONE-1 and CNE-1 cells treated with 0 and 30 μM Sch B. (**B**) Molecular docking of Sch B binding to CDK4 and CDK6.

B + 4 Gy group cells (Mean values for γ-H2AX foci/nucleus: HONE-1 21.4, CNE-1 19.7) markedly elevated than that of the 4 Gy radiation group (Mean values for γ-H2AX foci/nucleus: HONE-1 13.2, CNE-1 12.5), indicating that Sch B promoted radiation-induced DNA damage. After 12 h of radiation, the positivity of γ-H2AX was extremely low in the 4 Gy radiation group (Mean values for γ-H2AX foci/nucleus: HONE-1 3.9, CNE-1 3.5), while the positivity of γ-H2AX in the Sch B + 4 Gy group (Mean values for γ-H2AX foci/nucleus: HONE-1 7.6, CNE-1 7.8) was significantly higher than that in the 4 Gy group, indicating that Sch B has the effect of delaying radiation damage repair in NPC.

Tumor organoids are 3D models in vitro, which can better simulate the structure of tumors compared to 2D cell lines. Previous studies have confirmed that 3D tumor model is a better former for studying radiosensitivity[27]. Therefore, we further validated the radiosensitization effect of Sch B on NPC using HONE-1 organoid model. The IC50 concentration of Sch B on HONE-1 organoids and the organoids' viability after different radiation doses were first determined (Fig. 5G,H), based on which, the subsequent combined treatment experiment selecting a Sch B concentration of 20 μM and a radiation dose of 12 Gy. After 6 days of combined treatment with Sch B and radiation, cell viability of organoids was tested (Fig. 5I,J). Compared with 12 Gy radiation group, the activity of HONE-1 organoids in the Sch B + 12 Gy group was significantly reduced, indicating that Sch B has a radiosensitization effect, which was consistent with the 2D system.

Discussion

The etiology of NPC is multifactorial, encompassing genetic predispositions, viral infections, environmental factors, and lifestyle choices[1,28–30]. Due to the concealment of anatomical location and no special clinical symptoms, the disease is often found at a late stage. The effect of radiation therapy for locally advanced NPC is poor, and comprehensive treatment is often used[31]. Comprehensive treatment of NPC includes induction chemotherapy, synchronous radiotherapy, adjuvant radiotherapy, targeted therapy and immunotherapy[32,33]. Induction chemotherapy commonly uses cisplatin, 5-FU and gemcitabine to reduce tumor load and enhance radiosensitivity[32]. Synchronized radiotherapy is the use of small doses of chemotherapeutic agents in parallel with radiotherapy, commonly used drugs are cisplatin, carboplatin, and Lobaplatin[34,35]. However, systemic chemotherapeutic agents may lead to local and systemic side effects and are less well-tolerated to patients. Therefore, it is urgent to explore agents that are non-toxic or low-toxic to normal human tissues as radiosensitizers. Sch B emerges as a potential candidate in this context, demonstrating efficacy in inhibiting NPC cell proliferation and sparing normal nasopharyngeal epithelial cells by modulating the cell cycle and enhancing radiosensitivity through the delayed repair of radiation-induced DNA damage.

Since the discovery of Sch B for more than 40 years, research on it have mainly focused on its anti-inflammatory, antioxidant and anti-fibrotic effects[36]. In recent years, the antitumor effects of Sch B have been highly anticipated[6]. The antitumor mechanisms of Sch B mainly include blocking the tumor cell cycle[6,17], inhibiting tumor cell invasion and metastasis, reducing the expression of p-glycoprotein, multidrug resistance protein 1 and reversing tumor multidrug resistance[37], inhibiting tumor angiogenesis[38] and tumor cell DNA synthesis, DNA damage repair[39,40]. However, the effect of Sch B and its related mechanisms in NPC has not been

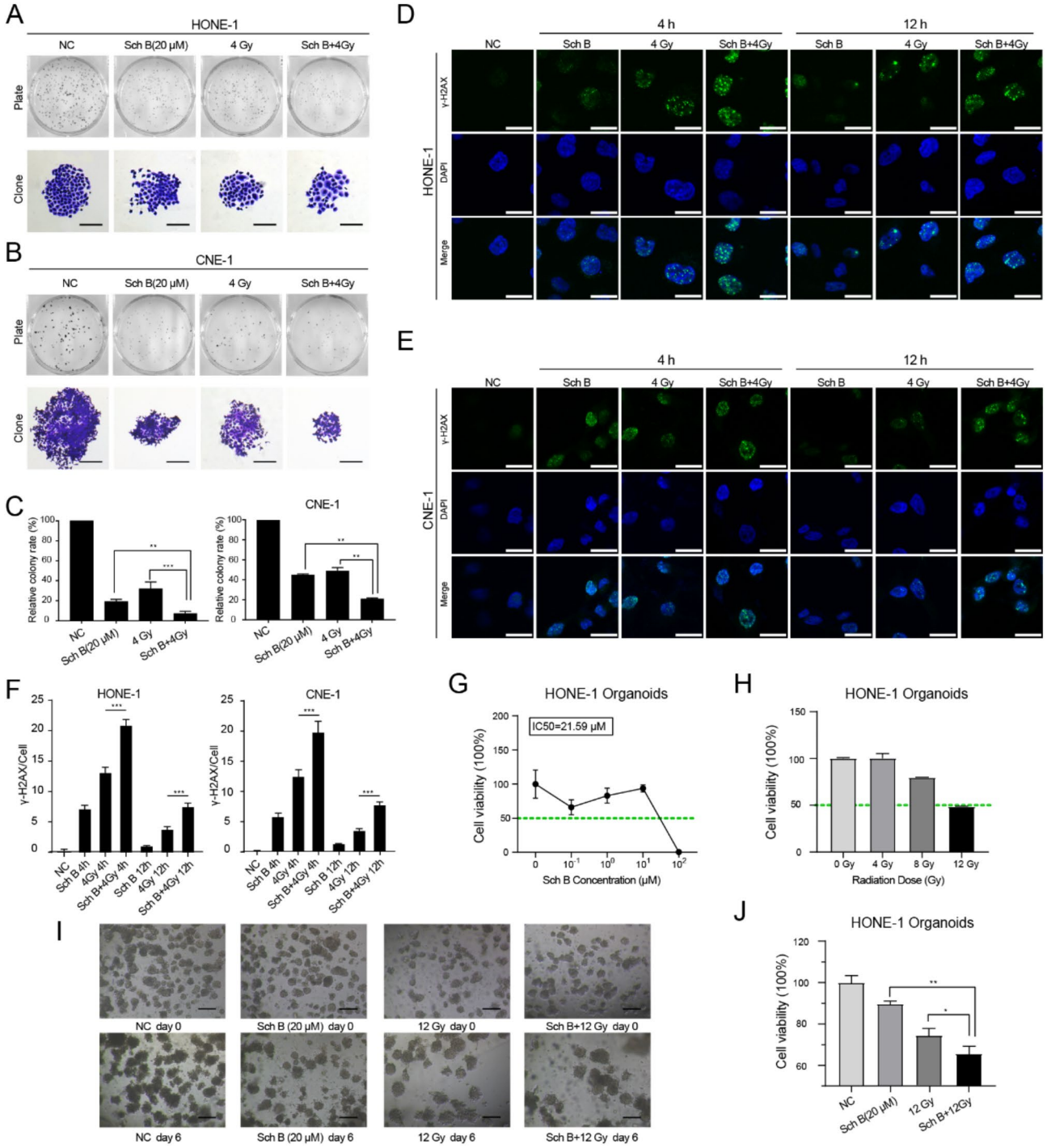

Fig. 5. Sch B increases the sensitivity of NPC cells to radiation. (**A**,**B**) Colony forming assay for HONE-1 and CNE-1 cells treated with Sch B (20 μM), radiation (4 Gy), Sch B+ radiation (20 μM + 4 Gy). (**C**) The formation rates of HONE-1 and CNE-1 cells treated with the conditions of (**A**,**B**). (**D**,**E**) Effect of Sch B or radiation on γ-H2AX foci formation for HONE-1 and CNE-1 cells. The representative images of nuclei from each group. Scale bar 20 μm. (**F**) Histogram represented values for γ-H2AX foci/nucleus. $^{*}P<0.05$; $^{**}P<0.01$; $^{***}P<0.001$. (**G**) The cell viability of HONE-1 organoids with different concentrations of Sch B. (**H**) The cell viability of HONE-1 organoids with different radiation dose. (**I**) Bright field images of HONE-1 organoids treated with Sch B, radiation, Sch B combined with radiation on day 0 and day 6. Scale bar 200 μm (**J**) The cell viability of HONE-1 organoids treated with Sch B, radiation, Sch B combined with radiation on day 6. $^{*}P<0.05$; $^{**}P<0.01$; $^{***}P<0.001$.

reported so far to our knowledge. This study marks the inaugural exploration of Sch B in the context of NPC, revealing its targeted inhibition of CDK4/6, consequent G1 phase arrest, and enhancement the radiosensitivity of NPC.

The sensitivity of tumor cells to radiation varies depending on different phases of the cell cycle. Generally, cells in the M and G2 phases are the most sensitive to radiation, followed by those in the G1 phase. When cells enter the S phase, they develop radiation resistance[41,42]. CDK4 and CDK6 are pivotal in driving cell cycle progression from G1 to S phase, with their activation facilitated by cyclin D upregulation in response to extracellular signals[43]. The phosphorylation of retinoblastoma protein (RB) by the CDK4/CDK6/cyclin D1 complex is a critical step in S phase entry[44,45]. In our study, western blot results showed that the expression of CDK4/6 was significantly reduced after Sch B on NPC cells. Through cyclin D1 increased, the ability to form CDK4/CDK6/Cyclin D1 complexes was reduced, leading to cell arrest in the G1 phase, which is consistent with the results of flow cytometry assay. Specifically, Sch B causes NPC cells to arrest in the G1 phase, a stage that exhibits heightened sensitivity to radiation. It impedes these cells from progressing into the S phase, during which cells demonstrate significant resistance to radiation. Thus, Sch B enhances the radiosensitivity of NPC cells. In a study of Sch B inhibiting lung cancer cells, it has also been confirmed that Sch B reduced CDK4/6 and Cyclin D1 expression, blocking cells in the G0/G1 phase[15]. The study of gallbladder cancer showed CDK4 down-regulation and G1 phase arresting[17]. Different from these studies, we also found that Sch B had little effect on the cell cycle and CDK4/6 of NP69. Furthermore, DNA double-strand breaks represent a primary consequence of radiation-induced damage. γ-H2AX, a well-established biomarker for DNA double-strand lesions, was utilized to investigate the impact of Sch B on DNA damage repair. We demonstrated that Sch B enhances radiosensitivity by delaying the repair of DNA damage.

After verifying that Sch B downregulates CDK4 and CDK6, we provided evidence that Sch B can directly interact with CDK4/6 using CETSA. However, based on the current data from this study and the existing literature on the anti-tumor effects of Sch B, the underlying mechanisms by which Sch B's targeting of CDK4 and CDK6 impacts the expression of these proteins remain elusive. In a study, nano-PROTACs were employed to specifically target and bind to CDK4/6. PROTACs recruit the intracellular ubiquitin–proteasome system, attach ubiquitin tags to CDK4/6, and then CDK4/6 is recognized and degraded by the proteasome[46]. It is possible that Sch B exerts its effect on the expression of CDK4/6 through a similar mechanism of degradation after binding.

CDK4/6 highly specific inhibitors include palbociclib (PD0332991), ribociclib (LEE011), and abemaciclib (LY2835219). Food and Drug Administration (FDA) has approved palbociclib and ribociclib for the treatment of HR-positive, HER2-negative advanced or metastatic breast cancer[47]. Clinical studies have found that CDK4/6 inhibitors have significant efficacy and stabilizing effects on solid tumors such as breast cancer and non-small cell lung cancer[47,48]. Among these selective inhibitors, palbociclib was the most widely investigated and has been evaluated both in vitro and in vivo[49,50]. Interestingly, palbociclib has been reported to amplify the radiosensitivity to NPC via mediating apoptosis and suppressing DNA damage repair[51]. Our results confirmed that Sch B targeted CDK4/6 and enhanced the sensitivity of NPC to radiotherapy, which have significant similarities with palbociclib. However, palbociclib has some common side effects include neutropenia, leukopenia, diarrhea, fatiue, peripheral neuropathy and dry eyes syndrome[52,53]. From this perspective, Sch B is superior to palbociclib. Multiple studies have confirmed that Sch B has no damage on normal tissues and organs at dozens of μM concentrations at the cellular and animal levels, and even has a protective effect on tissues and organs[9,54,55]. Sch B has been documented in previous research to exhibit antioxidant properties within hepatocytes[56]. Oxidative stress is a well-recognized primary contributor to DNA damage. Reactive oxygen species (ROS), which are not only generated endogenously under normal physiological stress but also can be produced during radiation treatments[57], are potent inducers of DNA lesions. Sch B can potentially reduce the oxidative damage to DNA in normal epithelial cells.

The complexity of Chinese medicine is often characterized by multiple effects, multiple targets, and multiple pathways of one drug. Sch B as the main active component of the Chinese medicine Schisandra Chinensis may have multiple antitumor effects as well as potential targets. However, we have confirmed that it does not cause damage to normal tissue cells. Therefore, Sch B may be a potential approach for the treatment of NPC. The present study was limited to the cellular and organoid levels, and on the effects of immune system and tumor microenvironment on the antitumor effects of Sch B in animal models are required for further validation.

Methods

Cell culture

The immortalized nasopharyngeal epithelial cell line NP69 and nasopharyngeal carcinoma cell lines HONE-1 and CNE-1 were gifted by the South China State Key Laboratory of Oncology, Cancer Prevention and Treatment Center of Sun Yat-sen University (passage 20). NP69 was cultured in Defined Keratinocyte-SFM medium (Gibco, 10744019) supplemented with 5% fetal bovine serum (PAN Seratech, ST30-3302) and 0.2% Defined Keratinocyte-SFM Growth Supplement. HONE-1 and CNE-1 were cultured in RPMI 1640 (Gibco, C11875500BT) medium containing 10% fetal bovine serum. All the cell lines were incubated in 5% CO_2, 37 °C.

CCK-8 cytotoxicity-proliferation assay

NP69 was seeded in 96-well plates at 4000 cell per well. HONE-1 and CNE-1 were inoculated in 96-well plates at 800 and 1000 cell per well, respectively. After the cells adhering to the wall, different concentrations of Sch B (0, 20, 40, 60, 80 and 100 μM) were added to each group and incubated for 24 h, 48 h, 72 h. Then, these cells were incubated with 100 μL medium and 10 μL CCK-8 reagent (New Cell and Molecular Biotech, C6005) at 37 °C for 2 h. The optical density (OD) value was read on microplate reader (BIO-RAD, CA, USA).

Colony formation assay

Proliferation inhibition effect of Sch B on NPC cells

The Sch B treated groups (10, 20, 30 and 40 μM) and the control group (0 μM) cells were planted in 6-well plates at 400 cell per well. After 7 d of culture, the colonies were fixed with 4% paraformaldehyde (BBI, E672002-0100) for 15 min, and were dyed with 0.1% crystal violet solution (BBI, 548-62-9) for 30 min, then photographed.

Radiosensitivity amplifying effect of Sch B on NPC cells

The control group (0 μM, 0 Gy), Sch B (Selleck, S3600) group (20 μM), radiation group (4 Gy), and Sch B combined radiation group (20 μM + 4 Gy) cells were planted in 6-well plates at 400 cell per well. The cells of Sch B group and Sch B combined radiation group were pretreated with 20 μM for 6 h. Then, the cells in each group were digested with trypsin, and irradiated the cells of radiation group and the Sch B combined radiation group with X-ray doses of 4 Gy, 6 Mv energy, 600 cGy/min. Cells of each group were re-seeded into 6-well plates. After 5 d of culture, perform the above steps for fixation, staining, and photography.

Organoid culture

Cell suspension was mixed with Matrigel (Corning, 356237) at the ratio 1:1 (vol/vol). 50 μL droplets of Matrigel-cell suspension droplets were added to a pre-heated 24-well plate. After gelation, 500 μL organoid medium (detailed composition seen Table S1) was gently added to each well. When conducting drug sensitivity experiment, 1 mL per well of Corning Cell Recovery Solution (Corning, 354253) was added to each well, incubating for 10 min at 37 °C, followed by centrifugated at 800 rpm. The organoids in radiation group (12 Gy), and Sch B combined radiation (20 μM + 12 Gy) were irradiated with X-ray doses of 12 Gy, 6 Mv energy, 600 cGy/min. Then, the organoids in each group were suspended in 50% cold Matrigel and reseeded in 96-well plates as described above. The organoids in Sch B group (20 μM) and Sch B combined radiation group (20 μM + 12 Gy) were treated with 20 μM Sch B, and new medium containing Sch B was changed at day 3. Six days after the Sch B and radiation exposure, ATP levels were measured using the CellTiter-Glo 3D Viability Assay (Promega, Cat# G9683) and luminescence was measured. Results were normalized to the control group (0 μM, 0 Gy).

Flow cytometry

HONE-1, CNE-1 and NP69 cells were divided into control group and Sch B treated group (10, 20, 30, and 40 μM). After 48 h of Sch B treatment, the cells were harvested. 3 mL of precooled 70% ethanol was dripped into the centrifuge tube and fixed overnight at − 20 °C. The fixed cells were centrifuged at 1500 rpm for 20 min and then washed with PBS, and then centrifuged with another 1500 rpm for 5 min. 5×10^5 cells were counted by ice-cold PBS suspension. 250 μL PI/RNase (Roche, Shanghai, China) was added, following by incubation in dark at room temperature for 15 min. After screening, cell cycle distribution was analyzed by a BD flow cytometer (Franklin Lakes, NJ, USA).

Transcriptome sequencing and differential expression analysis

We prepared samples of HONE-1, HONE-1-SchB, NP69, and NP69-SchB to send to the Beijing Genomics Institute (BGI) for sequencing (Drug effects for 48 h), and sequencing was repeated three times. The RNA libraries were sequenced with PE 150 bp using BGISEQ platform. Raw reads are filtered by SOAPnuke and clean reads were compared to the reference sequence GRCh37 through HISAT. Gene quantitative analysis, various analyses based on gene expression levels were conducted, and the differentially expressed genes among the selected samples were further explored and analyzed through KEGG path significance enrichment analysis.

Molecular docking

The structural data format for Sch B was accessed through PubChem (https://pubchem.ncbi.nlm.nih.gov/), and the PDB (Protein Data Bank) format for CDK4 and CDK6 were accessed through PDB (https://www.rcsb.org/). Active ingredients and targets were pretreated: Sch B was fully hydrogenated, set to ligand automatically distributed charge and macromolecular proteins were dehydrated, fully hydrogenated by PyMOL, Autodock4.2.6. Molecular docking of compounds and core targets was performed using autodock-tools1.5.7 software, and the lowest energy binding mode was mapped using PyMOL.

Western blot

The total protein was extracted from RIPA lysate (Sangon, C500005-0100), denatured, and concentrated into 20 μg for each sample. It was separated by 10% SDS-PAGE electrophoresis and transferred to the PVDF membrane. The PVDF membrane was sealed with 5% skim milk at room temperature for 1 h, then incubated overnight at 4 °C with an antibody CDK4 (Proteintech, Illinois, USA, Cat. No. 11026-1-AP, 1:2000), CDK6 (CST, Cat. No. 13331S, 1:1000), Cyclin D1 (CST, Cat. No. 2978S, 1:1000), and GAPDH (CST, Cat. No. 5174S, 1:8000). The membrane was washed with TBS-T for 10 min for 3 times the next day, and incubated with goat anti-rabbit second antibody (1: 10,000) at room temperature for 1 h. After washing with TBS-T for 10 min for 3 times, proteins were visualized with electrochemiluminescence substrate (Advansta, California, USA). The strips were photographed and analyzed by Tanon-5200 automatic chemiluminescence imaging analysis system (Tanon, Shanghai, China).

Cellular thermal shift assay

The experiment was divided into Sch B treated group (30 μM) and control group (0 μM), cells in each group were seeded into two plates of 10 cm dish. After being treated with Sch B for 4 h, the cells were collected and re-suspended with PBS containing PI and PPI. The cell suspension was frozen and thawed rapidly in liquid nitrogen and 37 °C water and repeated for 3 times. After centrifugation at 13,000 rpm for 20 min, the supernatant was

placed in 0.2 mL EP tubes averagely. The EP tube is rapidly heated by PCR instrument, the temperature range is 43–64 °C. After heating for 3 min, the temperature was reduced to 20 °C. The fully denatured protein was used in protein immunoblotting experiment.

Immunofluorescence assay

Cells were seeded on coverslips in a 24-well plate, then treated with Sch B for 4 h and exposed to a radiation dose of 4 Gy. They were fixed with 4% paraformaldehyde for 15 min at 4 and 12 h post radiation, and blocked in 5% BSA for 1 h at room temperature. Then, the cells were incubated with γ-histone-H2AX antibody (CST, Cat. No.2577s,1:300) and overnight at 4 °C, followed by incubation with Alexa488 antibody (Abbkine, Cat. No. a23210, 1:200) for 1 h at room temperature. The coverslips were stained with DAPI for 15 min to visualize nuclei. Images were captured with fluorescent confocal microscopy (Olympus Optical Co., Tokyo, Honshu, Japan).

Statistical analysis

GraphPad Prism 8.4.3 was used to analyze the data. Each experiment was repeated at least three times. The data are expressed as mean ± standard deviation. Statistical analysis was performed by Student's t test to detect the significant differences between two groups. P value < 0.05 was considered as statistically significant.

Data availability

All data generated or analyzed during this study are included in this published article. The original data supporting these findings are available at any time upon request to the corresponding author.

Received: 19 July 2024; Accepted: 4 March 2025
Published online: 12 March 2025

References

1. Chen, Y. P. et al. Nasopharyngeal carcinoma. *Lancet* **394**, 64–80. https://doi.org/10.1016/S0140-6736(19)30956-0 (2019).
2. Shao, K. et al. A detailed dosimetric comparative study of IMRT and VMAT in normal brain tissues for nasopharyngeal carcinoma patients treated with radiotherapy. *Front. Radiol.* **3**, 1190763. https://doi.org/10.3389/fradi.2023.1190763 (2023).
3. He, H. et al. Overexpression of beta-catenin decreases the radiosensitivity of human nasopharyngeal carcinoma CNE-2 cells. *Cell. Physiol. Biochem.* **50**, 1929–1944. https://doi.org/10.1159/000494873 (2018).
4. Komorowska, D., Radzik, T., Kalenik, S. & Rodacka, A. Natural radiosensitizers in radiotherapy: Cancer treatment by combining ionizing radiation with resveratrol. *Int. J. Mol. Sci.* **23**, 10627. https://doi.org/10.3390/ijms231810627 (2022).
5. Calvaruso, M. et al. Nutraceutical compounds as sensitizers for cancer treatment in radiation therapy. *Int. J. Mol. Sci.* **20**, 5267. https://doi.org/10.3390/ijms20215267 (2019).
6. Nasser, M. I. et al. A comprehensive review on Schisandrin B and its biological properties. *Oxid. Med. Cell. Longev.* **2020**, 2172740. https://doi.org/10.1155/2020/2172740 (2020).
7. Cai, Z., Liu, J., Bian, H., Cai, J. & Zhu, G. Suppression of P2X7/NF-κB pathways by Schisandrin B contributes to attenuation of lipopolysaccharide-induced inflammatory responses in acute lung injury. *Arch. Pharm. Res.* **39**, 499–507. https://doi.org/10.1007/s12272-016-0713-0 (2016).
8. Shi, H. et al. Schisandrin B antagonizes cardiotoxicity induced by pirarubicin by inhibiting mitochondrial permeability transition pore (mPTP) opening and decreasing cardiomyocyte apoptosis. *Front. Pharmacol.* **12**, 733805. https://doi.org/10.3389/fphar.2021.733805 (2021).
9. Fang, Y., Zhang, L., Wang, Z., Wang, R. & Liang, S. Potential protective benefits of Schisandrin B against severe acute hepatitis in children during the COVID-19 pandemic based on a network pharmacology analysis. *Front. Pharmacol.* **13**, 969709. https://doi.org/10.3389/fphar.2022.969709 (2022).
10. Li, J. et al. Schisandrin B prevents ulcerative colitis and colitis-associated-cancer by activating focal adhesion kinase and influence on gut microbiota in an in vivo and in vitro model. *Eur. J. Pharmacol.* **854**, 9–21. https://doi.org/10.1016/j.ejphar.2019.03.059 (2019).
11. Nasser, M., Han, T., Adlat, S., Tian, Y. & Jiang, N. Inhibitory effects of Schisandrin B on human prostate cancer cells. *Oncol. Rep.* https://doi.org/10.3892/or.2018.6791 (2018).
12. Dai, X. et al. Schisandrin B exhibits potent anticancer activity in triple negative breast cancer by inhibiting STAT3. *Toxicol. Appl. Pharmacol.* **358**, 110–119. https://doi.org/10.1016/j.taap.2018.09.005 (2018).
13. Wang, S. et al. Schisandrin B reverses doxorubicin resistance through inhibiting P-glycoprotein and promoting proteasome-mediated degradation of survivin. *Sci. Rep.* **7**, 8419. https://doi.org/10.1038/s41598-017-08817-x (2017).
14. He, X. et al. Chinese medicine Bu-Fei decoction attenuates epithelial–mesenchymal transition of non-small cell lung cancer via inhibition of transforming growth factor β1 signaling pathway in vitro and in vivo. *J. Ethnopharmacol.* **204**, 45–57. https://doi.org/10.1016/j.jep.2017.04.008 (2017).
15. Lv, X. et al. Schisandrin B inhibits the proliferation of human lung adenocarcinoma A549 cells by inducing cycle arrest and apoptosis. *Int. J. Clin. Exp. Med.* **8**, 6926–6936 (2015).
16. Li, Q. et al. Antiproliferative and apoptosis-inducing activity of schisandrin B against human glioma cells. *Cancer Cell Int.* **15**, 12. https://doi.org/10.1186/s12935-015-0160-x (2015).
17. Xiang, S. S. et al. Schisandrin B induces apoptosis and cell cycle arrest of gallbladder cancer cells. *Molecules* **19**, 13235–13250. https://doi.org/10.3390/molecules190913235 (2014).
18. Wu, Y. et al. Down-modulation of heat shock protein 70 and up-modulation of Caspase-3 during schisandrin B-induced apoptosis in human hepatoma SMMC-7721 cells. *World J. Gastroenterol.* **10**, 2944–2948. https://doi.org/10.3748/wjg.v10.i20.2944 (2004).
19. Nasser, M. I. et al. A comprehensive review on schisandrin B and its biological properties. *Oxid. Med. Cell. Longev.* https://doi.org/10.1155/2020/2172740 (2020).
20. Li, L., Lu, Q., Shen, Y. & Hu, X. Schisandrin B enhances doxorubicin-induced apoptosis of cancer cells but not normal cells. *Biochem. Pharmacol.* **71**, 584–595. https://doi.org/10.1016/j.bcp.2005.11.026 (2006).
21. He, L. et al. Schisandrin B suppresses gastric cancer cell growth and enhances the efficacy of chemotherapy drug 5-FU in vitro and in vivo. *Eur. J. Pharmacol.* **920**, 174823. https://doi.org/10.1016/j.ejphar.2022.174823 (2022).
22. Yan, C., Gao, L., Qiu, X. & Deng, C. Schisandrin B synergizes docetaxel-induced restriction of growth and invasion of cervical cancer cells in vitro and in vivo. *Ann. Transl. Med.* **8**, 2305–5839. https://doi.org/10.21037/atm-20-6109 (2020).
23. Kanehisa, M.A.-O.X., Furumichi, M., Sato, Y., Matsuura, Y. & Ishiguro-Watanabe, M. KEGG: Biological systems database as a model of the real world. *Nucleic Acids Res.* **53**, D672–D677. https://doi.org/10.1093/nar/gkae909 (2025).

24. Kanehisa, M.A.-O.X. Toward understanding the origin and evolution of cellular organisms. *Protein Sci.* **28**, 1947–1951. https://doi.org/10.1002/pro.3715 (2019).
25. Kanehisa, M. & Goto, S. KEGG: Kyoto encyclopedia of genes and genomes. *Nucleic Acids Res.* **28**, 27–30. https://doi.org/10.1093/nar/28.1.27 (2000).
26. Martinez Molina, D. et al. Monitoring drug target engagement in cells and tissues using the cellular thermal shift assay. *Science* **341**, 84–87. https://doi.org/10.1126/science.1233606 (2013).
27. Yanhua, F. et al. Extracellular matrix stiffness mediates radiosensitivity in a 3D nasopharyngeal carcinoma model. *Cancer Cell Int.* **22**, 364. https://doi.org/10.1186/s12935-022-02787-5 (2022).
28. Chang, E. T., Ye, W., Zeng, Y. X. & Adami, H. O. The evolving epidemiology of nasopharyngeal carcinoma. *Cancer Epidemiol. Biomark. Prev.* **30**, 1035–1047. https://doi.org/10.1158/1055-9965.Epi-20-1702 (2021).
29. Lee, H. M., Okuda, K. S., González, F. E. & Patel, V. Current perspectives on nasopharyngeal carcinoma. *Adv. Exp. Med. Biol.* **1164**, 11–34. https://doi.org/10.1007/978-3-030-22254-3_2 (2019).
30. Goshtasbi, K. et al. A comprehensive analysis of treatment management and survival outcomes in nasopharyngeal carcinoma. *Otolaryngol. Head Neck Surg.* **165**, 93–103. https://doi.org/10.1177/0194599820973241 (2021).
31. Guan, S., Wei, J., Huang, L. & Wu, L. Chemotherapy and chemo-resistance in nasopharyngeal carcinoma. *Eur. J. Med. Chem.* **207**, 112758. https://doi.org/10.1016/j.ejmech.2020.112758 (2020).
32. Lee, V. et al. Palliative systemic therapy for recurrent or metastatic nasopharyngeal carcinoma—How far have we achieved?. *Crit. Rev. Oncol. Hematol.* **114**, 13–23. https://doi.org/10.1016/j.critrevonc.2017.03.030 (2017).
33. Ni, M. et al. Induction chemotherapy combined with intensity-modulated radiotherapy for 129 nasopharyngeal carcinoma patients with synchronous metastases: A retrospective study. *Front. Oncol.* **11**, 654871. https://doi.org/10.3389/fonc.2021.654871 (2021).
34. Lv, X. et al. Induction chemotherapy with lobaplatin and fluorouracil versus cisplatin and fluorouracil followed by chemoradiotherapy in patients with stage III–IVB nasopharyngeal carcinoma: An open-label, non-inferiority, randomised, controlled, phase 3 trial. *Lancet Oncol.* **22**, 716–726. https://doi.org/10.1016/s1470-2045(21)00075-9 (2021).
35. Sun, L. et al. ATP-responsive smart hydrogel releasing immune adjuvant synchronized with repeated chemotherapy or radiotherapy to boost antitumor immunity. *Adv. Mater. (Deerfield Beach, Fla.)* **33**, e2007910. https://doi.org/10.1002/adma.202007910 (2021).
36. Mou, Z. et al. Schisandrin B alleviates diabetic nephropathy through suppressing excessive inflammation and oxidative stress. *Biochem. Biophys. Res. Commun.* **508**, 243–249. https://doi.org/10.1016/j.bbrc.2018.11.128 (2019).
37. Sun, M., Xu, X., Lu, Q., Pan, Q. & Hu, X. Schisandrin B: A dual inhibitor of P-glycoprotein and multidrug resistance-associated protein 1. *Cancer Lett.* **246**, 300–307. https://doi.org/10.1016/j.canlet.2006.03.009 (2007).
38. Li, X. Y. et al. Functional vinorelbine plus schisandrin B liposomes destroying tumor metastasis in treatment of gastric cancer. *Drug Dev. Ind. Pharm.* **47**, 100–112. https://doi.org/10.1080/03639045.2020.1862169 (2021).
39. Nishida, H. et al. Inhibition of ATR protein kinase activity by schisandrin B in DNA damage response. *Nucleic Acids Res* **37**, 5678–5689. https://doi.org/10.1093/nar/gkp593 (2009).
40. Thandavarayan, R. A. et al. Schisandrin B prevents doxorubicin induced cardiac dysfunction by modulation of DNA damage, oxidative stress and inflammation through inhibition of MAPK/p53 signaling. *PLoS ONE* **10**, e0119214. https://doi.org/10.1371/journal.pone.0119214 (2015).
41. Blakely, E. et al. Cell-cycle radiation response: role of intracellular factors. *Adv. Space Res.* **9**, 177–186. https://doi.org/10.1016/0273-1177(89)90436-5 (1989).
42. Qian, X. et al. Astaxanthin increases radiosensitivity in esophageal squamous cell carcinoma through inducing apoptosis and G2/M arrest. *Dis. Esophagus Off. J. Int. Soc. Dis. Esophagus* **30**, 1–7. https://doi.org/10.1093/dote/dox027 (2017).
43. Aktas, H., Cai, H. & Cooper, G. M. Ras links growth factor signaling to the cell cycle machinery via regulation of cyclin D1 and the Cdk inhibitor p27KIP1. *Mol. Cell. Biol.* **17**, 3850–3857. https://doi.org/10.1128/mcb.17.7.3850 (1997).
44. Hiebert, S. W., Chellappan, S. P., Horowitz, J. M. & Nevins, J. R. The interaction of RB with E2F coincides with an inhibition of the transcriptional activity of E2F. *Genes Dev.* **6**, 177–185. https://doi.org/10.1101/gad.6.2.177 (1992).
45. Zhang, Z., Golomb, L. & Meyerson, M. Functional genomic analysis of CDK4 and CDK6 gene dependency across human cancer cell lines. *Cancer Res.* **82**, 2171–2184. https://doi.org/10.1158/0008-5472.Can-21-2428 (2022).
46. Yang, L. et al. Sequential responsive nano-PROTACs for precise intracellular delivery and enhanced degradation efficacy in colorectal cancer therapy. *Signal Transduct. Target Ther.* **9**, 275. https://doi.org/10.1038/s41392-024-01983-1 (2024).
47. Xu, H. et al. Recent advances of highly selective CDK4/6 inhibitors in breast cancer. *J. Hematol. Oncol.* **10**, 97. https://doi.org/10.1186/s13045-017-0467-2 (2017).
48. Patnaik, A. et al. Efficacy and safety of abemaciclib, an inhibitor of CDK4 and CDK6, for patients with breast cancer, non-small cell lung cancer, and other solid tumors. *Cancer Discov.* **6**, 740–753. https://doi.org/10.1158/2159-8290.Cd-16-0095 (2016).
49. Fry, D. et al. Specific inhibition of cyclin-dependent kinase 4/6 by PD 0332991 and associated antitumor activity in human tumor xenografts. *Mol. Cancer Ther.* **3**, 1427–1438 (2004).
50. Toogood, P. et al. Discovery of a potent and selective inhibitor of cyclin-dependent kinase 4/6. *J. Med. Chem.* **48**, 2388–2406. https://doi.org/10.1021/jm049354h (2005).
51. Xie, X. et al. CDK4/6 inhibitor palbociclib amplifies the radiosensitivity to nasopharyngeal carcinoma cells via mediating apoptosis and suppressing DNA damage repair. *Onco Targets Ther.* **12**, 11107–11117. https://doi.org/10.2147/OTT.S234221 (2019).
52. Lai, J. et al. Clinical and genotypic insights into higher prevalence of palbociclib associated neutropenia in Asian patients. *Oncologist* https://doi.org/10.1093/oncolo/oyad304 (2023).
53. Al-Ziftawi, N. et al. The effectiveness and safety of palbociclib and ribociclib in stage IV HR+/HER-2 negative breast cancer: A nationwide real world comparative retrospective cohort study. *Front. Oncol.* **13**, 1203684. https://doi.org/10.3389/fonc.2023.1203684 (2023).
54. Zhu, S. et al. Protective effect of schisandrin B against cyclosporine A-induced nephrotoxicity in vitro and in vivo. *Am. J. Chin. Med.* **40**, 551–566. https://doi.org/10.1142/s0192415x12500425 (2012).
55. Zhang, W., Sun, Z. & Meng, F. Schisandrin B ameliorates myocardial ischemia/reperfusion injury through attenuation of endoplasmic reticulum stress-induced apoptosis. *Inflammation* **40**, 1903–1911. https://doi.org/10.1007/s10753-017-0631-4 (2017).
56. Pou Kuan, L., Po Yee, C., Na, C., Hoiyan, L. & Kam Ming, K. Schisandrin B elicits a glutathione antioxidant response and protects against apoptosis via the redox-sensitive ERK/Nrf2 pathway in AML12 hepatocytes. *Free Radic. Res.* **45**, 483–495. https://doi.org/10.3109/10715762.2010.550917 (2011).
57. Ji, W., Lee, M., Kim, G. & Kim, E. Quantitation of the ROS production in plasma and radiation treatments of biotargets. *Sci. Rep.* **9**, 19837. https://doi.org/10.1038/s41598-019-56160-0 (2019).

Acknowledgements

We would like to express our gratitude to the members of our laboratory for their insightful scientific discussions. This work was supported by the Health Commission of Dalian (Grant Number 22Z11004), the High-level Talent Innovation Support Program of Dalian Science and Technology Bureau (Grant Number 2021RD02), and the National Natural Science Foundation of China (Grant Number 82172822).

Author contributions

Yanhua Fang: Writing—review and editing, funding acquisition. Xinhui Lv: Project administration. Ge Li: Data curation, formal analysis. Piao Wang: Project administration, visualization. Lingling Zhang: Project administration, writing–original draft. Ruoyu Wang: Supervision, funding acquisition. Lingyun Jia: Conceptualization, supervision, investigation. Shanshan Liang: Conceptualization, supervision, investigation.

Declarations

Competing interests

The authors declare no competing interests.

Additional information

Supplementary Information The online version contains supplementary material available at https://doi.org/10.1038/s41598-025-92992-9.

Correspondence and requests for materials should be addressed to L.J. or S.L.

Reprints and permissions information is available at www.nature.com/reprints.

Publisher's note Springer Nature remains neutral with regard to jurisdictional claims in published maps and institutional affiliations.